EXTRACTING LINE FEATURES FROM SYNTHETIC APERTURE RADAR (SAR) SCENES USING A MARKOV RANDOM FIELD MODEL

Olaf Hellwich and Helmut Mayer*

Chair for Photogrammetry and Remote Sensing, Technical University Munich
Arcisstr. 21, D-80290 München, Germany
T: +49.89.2892.2677, F: +49.89.280.9573, EMail: olaf@photo.verm.tu-muenchen.de

ABSTRACT

Due to the speckle effect of coherent imaging the detection of lines in SAR scenes is considerably more difficult than in optical images. A new approach to detect lines in noisy images using a Markov random field (MRF) model and Bayesian classification is proposed. The unobservable object classes of single pixels are assumed to fulfill the Markov condition, i.e. to depend on the object classes of neighboring pixels only. The influence of neighboring line pixels is formulated based on potentials derived from a random walk model. Locally, the image data is evaluated with a rotating template. As SAR intensity data is deteriorated by multiplicative noise, the response of the local line detector is a normalized intensity ratio which results in a constant false alarm rate. The approach integrates intensity, coherence from interferometric processing of a SAR scene pair, and given Geographic Information System (GIS) data.

1. INTRODUCTION

The new approach for the extraction of linear structures is related to methods which combine local operators with a more global evaluation [1], as it is based on Bayesian inference and formulates prior knowledge about the continuity of lines as an MRF. To overcome the difficulties in the detection of linear structures the approach integrates generic knowledge about lines, given GIS data and the SAR scene data. The generic knowledge can be subdivided into three parts. The first part is the knowledge about the physical appearance of lines, i.e. narrow, elongated areas with approximately constant image intensity (see above). This type of knowledge is used to evaluate the scene data. In terms of Bayesian approaches it is therefore incorporated in the conditional probability density function (PDF) to observe scene data given a linear structure. The second part of knowledge about lines says that a line is continuous over a certain region of the scene. This means that a line can be assumed in a location where there is not enough physical evidence, if neighboring locations show sufficient evidence. This knowledge is the basis of a random walk model which is used in the prior PDF modeling the relationships between pixels of linear structures based on an MRF. In addition to the generic knowledge about the appearance of linear structures, the specific knowledge of the presence of a certain linear structure as given by a GIS is incorporated into the approach as third part of the knowledge.

* This research was partially funded by Deutsche Agentur für Raumfahrtangelegenheiten (DARA) GmbH under contract 50EE9423.

To solve the inverse problem of computing the location of lines from the measured scene data a Bayesian approach is applied [2]. The posterior probability density of the object parameters given the scene data is derived according to Bayes' theorem

$$p(\varepsilon|y) \propto p(y|\varepsilon) \cdot p(\varepsilon) \tag{1.1}$$

where ε is the object parameter vector, and y is the data vector. ε contains one element ε_s for each site $s \in S$, i.e. regularly for each pixel of the scene S. The object parameters as well as the scene data are assumed to be MRF. A random field is Markovian, if for all x

$$p(x_s|x_r, r \neq s) = p(x_s|\partial x_s) \tag{1.2}$$

where ∂x_s is a neighborhood of s considerably smaller than the complete scene [3], [4]. For the scene data, it is assumed that $\partial y_s = \{\}$, i.e. each data sample is independent of its neighbors. As the equivalence of MRF and neighborhood Gibbs fields is used, energy functions and clique potentials can be used instead of PDF. The scene data y is a vectorial MRF $y_s{}^T = (y_{I_s} \quad y_{C_s})$ where y_{I_s} and y_{C_s} are the intensity and the coherence, respectively. If y_{I_s} and y_{C_s} are considered as independent [5], the relation between data and prior knowledge can be expressed as [6]

$$H_s(\varepsilon_s|y_{I_s}, y_{C_s}, \partial\varepsilon_s) = H_s(y_{I_s}|\varepsilon_s) + H_s(y_{C_s}|\varepsilon_s) + H_s(\varepsilon_s|\partial\varepsilon_s) \tag{1.3}$$

The components of (1.3) are explained in detail in sections 2 and 3. A more comprehensive description of the approach is given in [7].

2. PRIOR KNOWLEDGE ABOUT LINEAR STRUCTURES

The model of continuous curvilinear structures was inspired by recent work about stochastic completion fields [8]. They describe occluded, but perceptually salient contours by random walks of particles having its source at unoccluded points of the contours. The path most probably taken by the particles is assumed to be the location of the illusory contour. We use a similar random walk model to derive the potentials of two-pixel cliques of a neighborhood Gibbs field. A neighboring line site t is treated as a source of random walks whereas the site s, i.e. in terms of MRF the site which is influenced by a neighbor and for which the energy is computed, serves as a sink. The more particles pass through s the higher is the probability that s is a line site.

A line or a migrating particle passing a site has more properties than only its quality of being a line or a line particle. Its path has a certain direction and curvature which can be estimated as well. Thus the state space $\boldsymbol{E}_S$ of the object parameters ε_S is

$$\mathbf{E}_S = \left\{ "no-line", "line(\theta_i, \kappa_j)" : i \in \{1,\mathrm{K}\, I\}, j \in \{1,\mathrm{K}\, J\} \right\} \quad (2.1)$$

where θ_i are I discrete directions equally spaced in the interval $[0,\pi[$, and κ_j are J discrete curvatures equally spaced in the interval $[-\kappa_{\max}, \kappa_{\max}]$ where $\kappa_{\max}$ is the magnitude of a maximum curvature.

The particles of the random walk originate at a certain position $P(x_0, y_0)$ in the x, y-coordinate plane and possess a direction θ_0 and a curvature κ_0. During each step of the random walks x, y, θ, and κ are updated. With each step a certain fraction of the particles decays. Fig. 2.1 shows an example of simulated random walks.

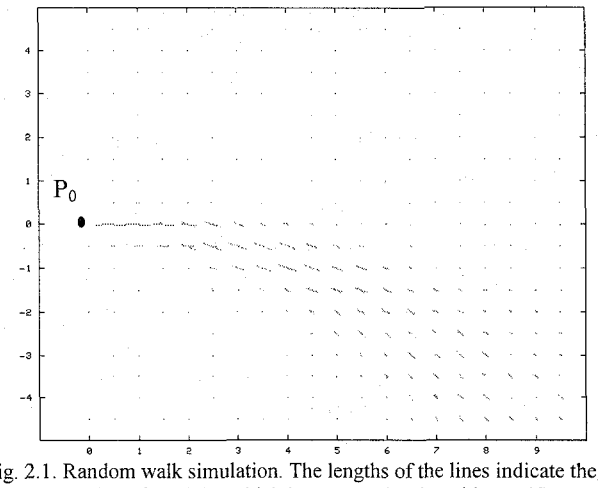

Fig. 2.1. Random walk simulation. The lengths of the lines indicate the number of particles which have passed a site with specific direction.

For the computation of the energies $H_s(\varepsilon_s|\partial\varepsilon_s)$ a neighborhood system of two-site cliques is defined. Each site has neighbors of varying order forming a clique with each of those neighbors. For an element ε_S of the state space $\boldsymbol{E}_S$, the counts of the random walk model are summed clique by clique. Each count depends on the parameter values ε_t and ε_S, i.e. on direction and curvature in the neighboring site t and the direction and curvature proposed at site s, as well as on the location of t with respect to s. If ε_t is "*no line*", the counts at s are *0* independent of ε_S. High counts for ε_S indicate a high probability of ε_S, as the presence of neighboring line sites support the presence of a line with the corresponding direction and curvature.

The neighborhood model is further extended, as a line should also make certain neighboring lines improbable. This is because line sites parallel to a directly neighboring line site do not conform with the elongatedness of lines. It can be modeled with the same type of random walks. We only imagine a different type of particles, called inhibiting particles, diffusing perpendicularly to the direction of a line site. The particles inhibit the presence of lines perpendicular to the direction of propagation in the same way the particles used before supported the presence of lines in the direction of propagation. Therefore, the corresponding counts make the presence of those lines improbable and are subtracted from the supporting counts.

Introducing a one-site clique containing only s, we can control the overall probability of a line independent from the state of neighboring sites.

Hence, in agreement with (1.3), $H_s(\varepsilon_s|\partial\varepsilon_s)$ is computed from

$$H_s(\varepsilon_s|\partial\varepsilon_s) = \begin{cases} -\ln(C) & \text{if } C \geq 1 \\ -\ln(1) & \text{if } C < 1 \end{cases} \quad (2.2)$$

$$C = C_{A_1}(\varepsilon_s) + \sum_{A_2} C_{A_2}(\varepsilon_s|\varepsilon_t; s,t \in A_2)$$

where C_{A_1} is the count-equivalent of the one-pixel clique:

$$C_{A_1}(\varepsilon_s) = \begin{cases} c_l & \text{if } \varepsilon_s = "line(\theta_s, \kappa_s)" \\ c_n & \text{if } \varepsilon_s = "no-line" \end{cases}$$

c_l and c_n are empirically chosen "basic currents" which control the overall probability of line and no-line sites. $\sum_{A_2} C_{A_2}$ is the sum of the counts of the two-site cliques containing s.

The proposed approach uses GIS data to support the extraction of linear structures. It may for instance be known that a road is crossing the imaged area, and an approximate registration of the SAR scene and the GIS data may be given. Around the projection of the road center line into the SAR scene the probability to detect a line with the direction and curvature of the road center line should be increased. These facts have to be used to compute the energy of the prior PDF. A corridor symmetrical around the object center line is defined inside of which the probability of the object class $\varepsilon_s = line(\theta_i, \kappa_i)$ is uniformly increased. θ_i and κ_i are the direction and curvature of the object center line at the point i closest to site s. The increase in probability is taken into account by changing the computation of C_{A_1} in (2.2) to

$$C_{A_1}(\varepsilon_s) = \begin{cases} c_l + c_c & \text{if } \varepsilon_s = "line(\theta_s, \kappa_s)" \wedge \\ & s \in corridor \wedge \theta_s = \theta_i \wedge \kappa_s = \kappa_i \\ c_l & \text{if } \varepsilon_s = "line(\theta_s, \kappa_s)" \text{ otherwise} \\ c_n & \text{if } \varepsilon_s = "no-line" \end{cases} \quad (2.3)$$

c_c is an "additional current" due to the presence of a GIS object.

3. LOCAL DATA EVALUATION

For edge detection in SAR intensity data the ratio edge detector has been shown to give the best measure of edge strength. It corresponds with the multiplicative noise characteristics of the data and results in a constant false alarm rate [9]. Therefore, this approach is also based on the ratio detector. In general it compares two small neighboring regions of the image. In each of the two regions the averages of the

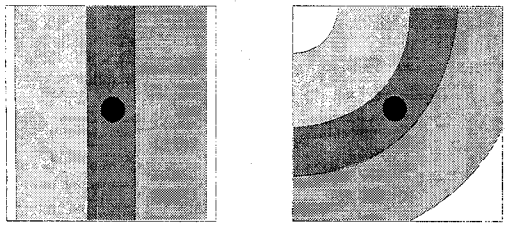

Fig. 3.1. Geometries of detector masks for line detection. The spot in the center of the window marks the site to be investigated.

intensities are computed. The normalized ratio is the ratio of the two averages using the larger one as the denominator.

To detect a line a detector mask is defined which consists of three regions [10]: a line region and two regions at the sides of the line region (see Fig. 3.1). Curved lines of varying widths can be considered.

The ratio operator is applied to all combinations of the detector mask regions. The line detector has to be prevented from giving a response to the location of edges or strong scatterers[10]. In case a line is present at the processed location the line region is homogenous, which means that the pixel intensities do not vary much. For SAR intensity data, this condition can be checked by computing the coefficient of variation

$$v_I = \frac{\sigma_I}{\langle I \rangle} \tag{3.1}$$

where $\langle I \rangle$ is the mean intensity and σ_I is the standard deviation of the intensity I. As $\sigma_I = I$ for homogenous regions, v_I of the investigated region has to be less than a threshold somewhat larger than 1 if the region does not contain any structures.

As the average values of the side regions may be influenced by the presence of strong scatterers, the median of the intensity values is computed. It is checked whether the line intensity differs significantly from the intensities of both side regions by computing the ratios between the line region and the side regions. These ratios are tested for membership in the PDF of the ratio of regions without contrast, i.e. regions which have the same intensities. For this purpose a threshold is derived from the PDF of the normalized ratio r for SAR intensity statistics [11]. Two regions are considered to be significantly different, if the ratio is smaller than 95% of the ratios computed from homogenous regions. If the line region is significantly different from both side regions, a line site has been found.

From the resulting ratio responses the energy values of the intensity data $H_s(y_{Is}|\varepsilon_s)$ are computed. Instead of the intensity of a pixel the ratio r_s is used to compute H_s, i.e.

$$H_s(y_{Is}|\varepsilon_s) = H_s(r_s|\varepsilon_s) \tag{3.2}$$

where r_s is a derived observation. The complete energy function of the intensity ratio is formulated as

$$H_s(r_s|\varepsilon_s) = \begin{cases} \dfrac{r_s^2}{2\sigma_r^2} & \text{if } s \text{ is a line site} \\ \dfrac{r_{\max}^2}{2\sigma_r^2} & \text{if } s \text{ is a no-line site} \end{cases} \tag{3.3}$$

where r_{max} and σ_r are empirically chosen values.

The coherence is processed in a similar manner as the intensity. The data is evaluated applying the same detector masks, but instead of the ratio the difference is computed. The checks for homogeneity, dissimilarity and similarity of regions are essentially the same as for intensity data except that the thresholds are derived more empirically, as the statistical properties of coherence data are not as well known as those of intensity data (but cf. [12]).

The estimation of the object parameters is conducted using simulated annealing as a stochastic or local highest confidence first (LHCF) estimation as a faster deterministic method [13].

4. RESULTS

A TOPSAR airborne data set consisting of intensity (Fig. 4.1) and coherence was evaluated. Fig. 4.2 shows the lines extracted from the intensity data. Many of the gaps have been closed even in locations where the ratio image does not show a significant response of the ratio line detector. This demonstrates the usefulness of the line model. Wide lines are not detected correctly as only detector masks for narrow lines were applied. Results comparing the use of intensita data with the combined use of intensity, coherence and GIS data are shown in [7].

Fig. 4.3 and 4.4 show that the approach is also suited for edge detection. In a satelliteborne SAR scene ridge lines, river banks and shadow boundaries have been detected.

5. CONCLUSIONS AND RECOMMENDATIONS

A new approach for the extraction of linear structures from SAR intensity and coherence data in a Bayesian framework using a MRF to model continuous curvilinearity was proposed. Results demonstrate the plausibility of the MRF line model.

Further tests of the approach are necessary. Presently, improvements regarding scale space integration are investigated. Scale space requirements can presently be met by using different line widths in the detector masks. A more effective way would be the use of an image pyramid or a multi-resolution MRF model [14]. We intend to make this topic subject of future publications.

ACKNOWLEDGMENTS

We thank Vexcel Corporation, Boulder, for providing the test data sets. Olaf Hellwich thanks John Curlander, Richard Carande and several other members of the Vexcel team for their support during his visit in Boulder.

REFERENCES

[1] Samadani R., Vesecky J. F. (1990): Finding Curvilinear Features in Speckled Images, IEEE Transactions on Geoscience and Remote Sensing, Vol. 28, No. 4, pp. 669-673.

[2] Oliver C. J. (1991): Information from SAR Images, J. of Physics D, Applied Physics, Vol. 24, No. 9, pp. 1493-1514.

[3] Geman S., Geman D. (1984): Stochastic Relaxation, Gibbs Distribution, and the Bayesian Restoration of Images, IEEE

Transactions on Pattern Analysis and Machine Intelligence, Vol. PAMI-6, No. 6, pp. 721-741.

[4] Winkler G. (1995): Image Analysis, Random Fields and Dynamic Monte Carlo Methods, Applications of Mathematics, Vol. 27, Springer-Verlag, Berlin.

[5] Hellwich O., Streck, C. (1996): Linear Structures in SAR Coherence Data, IGARSS '96, Lincoln, in press.

[6] Schistad Solberg A.H., Taxt T. (1994): Classification of Multisource Satellite Imagery Based on a Markov Random Field Model, Image and Signal Processing for Remote Sensing, Rome, SPIE Proc., Vol. 2315, pp. 322-331.

[7] Hellwich O., Mayer H., Winkler G. (1996): Detection of Lines in Synthetic Aperture Radar (SAR) Scenes, ISPRS Congress, Vienna, in press.

[8] Williams L.R., Jacobs D.W. (1995): Stochastic Completion Fields: A Neural Model of Illusory Contour Shape and Salience, 5th ICCV, Cambridge, pp. 408-415.

[9] Touzi R., Lopes A., Bousquet P. (1988): A Statistical and Geometrical Edge Detector for SAR Images, IEEE Transactions on Geoscience and Remote Sensing, Vol. 26, No. 6, pp. 764-773.

[10] Lopes A., Nezry E., Touzi R., Laur H. (1993): Structure Detection and Statistical Adaptive Speckle Filtering in SAR Images, Int. J. of Remote Sensing, Vol. 14, No. 9, pp. 1735-1758.

[11] Caves R.G. (1993): Automatic Matching of Features in Synthetic Aperture Radar Data to Digital Map Data, Ph.D. thesis, University of Sheffield, Dept. of Applied and Computational Mathematics.

[12] Tough R.J.A., Blacknell D., Quegan S. (1994): Estimators and Distributions in Single and Multi-Look Polarimetric and Interferometric Data, IGARSS '94, Pasadena, Electronical Digest.

[13] Chou P.B., Cooper P.R., Swain M.J., Brown C.M., Wixson L.E. (1993): Probabilistic Network Inference for Cooperative High and Low Level Vision, in: Chellappa R., Jain A., Markov Random Fields. Theory and Applications, Academic Press, Boston, pp. 211-243.

[14] Bouman C. A., Shapiro M. (1994): A Multiscale Random Field Model for Bayesian Image Segmentation, IEEE Transactions on Image Processing, Vol. 3, No. 2, pp. 162-177.

Fig. 4.1. Histogram-equalized amplitude of TOPSAR scene of 94/08/05.

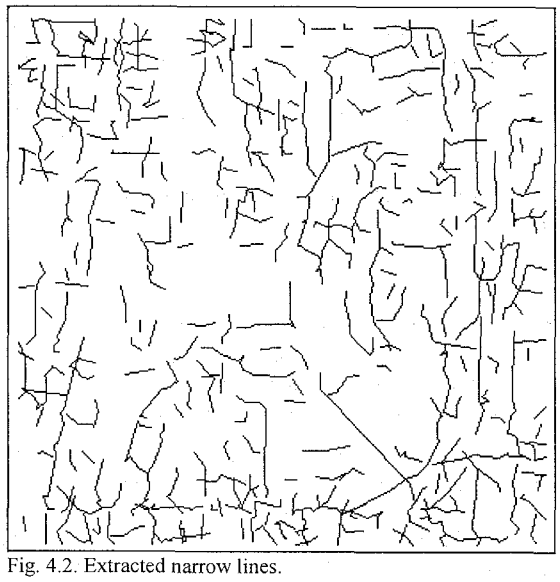

Fig. 4.2. Extracted narrow lines.

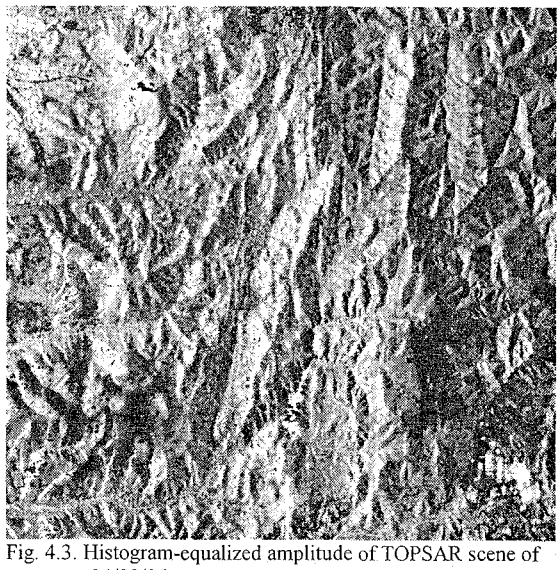

Fig. 4.3. Histogram-equalized amplitude of TOPSAR scene of 94/08/05.

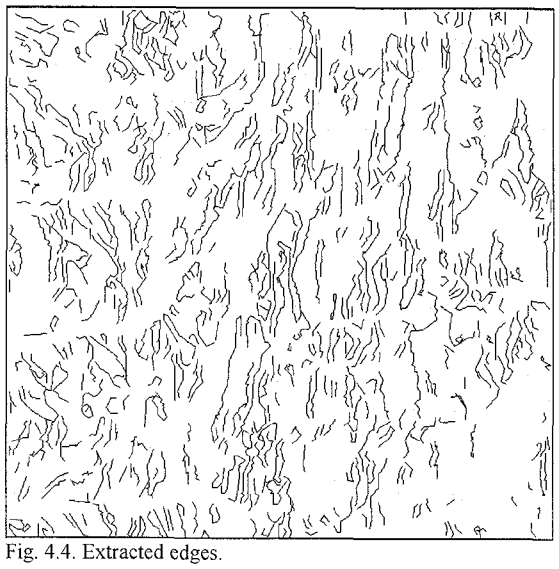

Fig. 4.4. Extracted edges.